# Journal of Materials Chemistry A

Accepted Manuscript


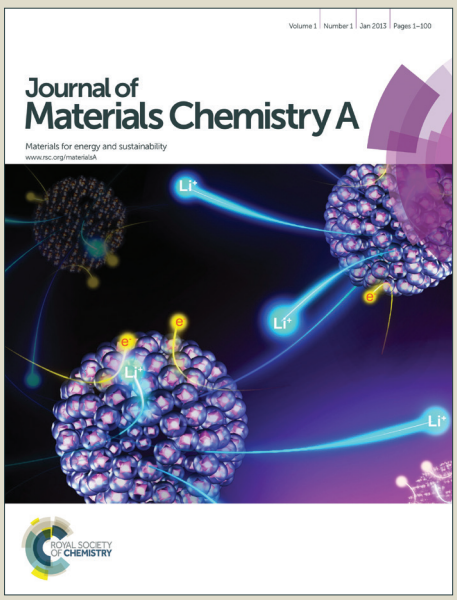





ROYAL SOCIETY OF CHEMISTRY

www.rsc.org/materialsA

**A table of contents entry.**

**Figure for TOC**

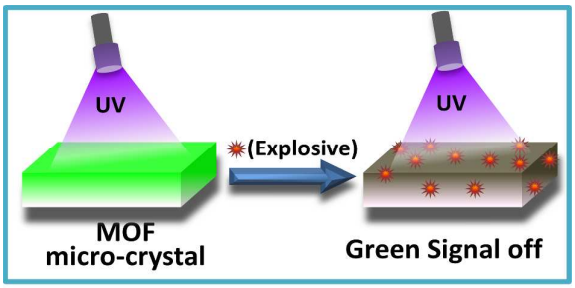


**Text for TOC**

Green emitting submicron sized metal-organic phosphor materials as a luminescence quenching based optical detector for explosive nitro aromatics in solution.

Journal Name

RSCPublishing

ARTICLE

# Optical Detection of Submicromolar level Nitro Explosives by a Submicron sized Metal-Organic Phosphor Material

Cite this: DOI: 10.1039/xoxxoooooox

Received ooth January 2012,
Accepted ooth January 2012

DOI: 10.1039/xoxxoooooox

www.rsc.org/

Debal Kanti Singha,[a] Saurav Bhattacharya,[b] Prakash Majee,[c] Sudip Kumar Mondal,*[c] Manoranjan Kumar,[a] and Partha Mahata*[a]

Two isomorphous submicron sized metal-organic network compounds, $[Y_2(PDA)_3(H_2O)_1].2H_2O$ (PDA = 1,4-Phenylenediacetate), **1** and $[Y_{1.8}Tb_{0.2}(PDA)_3(H_2O)_1].2H_2O$, **Tb@1** have been synthesized employing solvent assisted liquid grinding followed by heating at 180 °C for 10 min and washing with water. Single crystal X-ray data of bulk **1** confirmed three dimensional porous structure. The structure and morphology of **1** and **Tb@1** were systematically characterized by PXRD, TGA, DSC, IR, SEM and EDX analysis. Dehydrated **Tb@1** [**Tb@1′**] shows high intense visible green emission on the exposure of UV light. The green emission of **Tb@1′** were used for the detection of nitro explosives, such as 2,4,6-trinitrophenol (TNP), 1,3-dinitro benzene (DNB), 2,4-dinitro toluene (DNT), nitro benzene (NB), 4-nitro toluene (NT) in acetonitrile. The results show that the emission intensity of dehydrated **Tb@1′** can be quenched by all the nitro analytes used in the present work. Remarkably, **Tb@1′** exhibit high efficiency for TNP, DNB and DNT detections with $K_{SV}$ [$K_{SV}$ = quenching constant based on linear Stern-Volmer plot] values of 70920, 44000 and 35430 $M^{-1}$, respectively, which are highest value amongst known metal-organic materials. Using this material submicromolar level (≡ 0.18 ppm) detection of nitro explosives has been achieved.

## Introduction

The increased use of explosive materials in terrorism demands the development of simple, inexpensive and rapid detection methods for trace explosive materials in the field of homeland security, forensic applications and environmental implications.[1] Nitro aromatics such as 2,4,6-trinitrophenol (TNP), 2,4,6-trinitro toluene (TNT), 2,4,6-trinitro benzene (TNB), 2,4-dinitro toluene (DNT), 1,3-dinitro benzene (DNB) are common ingredients of explosives.[2] DNT and DNB are inevitable byproduct in the manufacturing process of TNT and TNB, respectively. Therefore, the detection of TNT and TNB explosives is often achieved by detection of DNT and DNB. TNP, on the other hand, is a powerful explosive and its explosive nature is even stronger that TNT.[3] TNP also cause unpleasant effects on human heath such as irritant to skin/eye and damage of respiratory system.[4] Therefore, the detection of such nitro aromatics is of high significance for explosive detections. Well trained canines or sophisticated instruments are currently used for the explosive detection though these are expensive and complex methods and have portability issues during in-field use.[5] Optical detections is gaining increasing attention due to its high simplicity, sensitivity and quick response time.[6] Recently luminescent metal-organic framework compounds, specially Zn and Cd based, have been emerged as new kind of materials for the detection of nitro explosive using the ligand centered luminescence.[7] The major disadvantage of ligand centered luminescence detectors are the small stokes shifts, which prevent to detect in naked eye as the differences of colour between emission and excitation light are very small. The lanthanides based metal-organic materials, especially $Eu^{3+}$ and $Tb^{3+}$, opened up another direction of explosive detection research based on their emission with large stokes shifts.[8] Metal-organic materials of these lanthanides ions generally shows unique luminescent through antenna effect where organic ligands function as sensitizer.[9] In this process, the organic ligands is excited to the singlet state, from which part of the energy is transferred to the triplet state through inter system crossing. The excited state transfer the energy to the metal centers, resulting a metal centered luminescence. Although few pure lanthanides based metal organic materials have been demonstrated for the detection of nitro explosives,[10] the easy naked eye detection is still an unexplored area as the pure lanthanide based metal-organic materials suffered from the self quenching.

Submicron/nano sized metal-organic materials has attracted considerable attentions, because these smaller materials possess superior properties and practical applicability's compared to their bulk counterparts in solubility, homogeneous disperse ability and adsorption kinetics.[11] Based on the above considerations, we chose a flexible aromatic dicarboxylate ligand, 1,4-phenylene diacetate (PDA), along with yttrium ions ($Y^{3+}$) for the construction of submicron sized host metal-organic material, $[Y_2(PDA)_3(H_2O)_1].2H_2O$ (PDA = 1,4-Phenylenediacetate), **1** and doping of 10% terbium ions ($Tb^{3+}$), in place of $Y^{3+}$, formed the desired phosphor material, **Tb@1**. The dehydrated **Tb@1** [**Tb@1′**] shows high intense visible green emission on the exposure of UV light. The luminescence of **Tb@1′** in acetonitrile show high sensitivity and quick visual detection ability toward the presence of trace amount of 2,4,6-

trinitrophenol (TNP), 1,3-dinitro benzene (DNB), 2,4-dinitro toluene (DNT) with respect of the luminescence quenching. It shows high sensitivity even in very low concentration region towards the detections of TNP, DNB and DNT with $K_{SV}$ (quenching constant) values 70920, 44000 and 35430 $M^{-1}$, respectively, which are amongst highest value known for metal-organic materials. Large value of $K_{SV}$ in presence of such low concentration of nitro explosives is a clear indication of strong molecular level interaction between sensor and analytes which ensures close proximity of sensor-analyte pair. This criterion makes our material more promising towards specific detection of nitro explosives in the submicromolar region.

This is the first observation, to our knowledge, where doping of lanthanide ion as activator in metal-organic material is used for the detection of nitro explosives and highest quenching constants for liquid phase detections of three explosive nitro compounds TNP, DNB and DNT is observed. In this article, we present the synthesis, structure and sensing behaviour of **1** and **Tb@1**.

## Experimental Section

### Materials

The chemicals needed for the synthesis of the metal-organic compounds, $Y(NO_3)_3.6H_2O$ (Sigma-Aldrich, 99.9%), $Tb(NO_3)_3.5H_2O$ (Sigma-Aldrich, 99.9%), 1,4-Phenylenediacetic acid, (Alfa Aesar, 97%), Ethanol (Merck, 99.9) were used as received. The chemical used for the detection experiments, acetonitrile (99.8%), 2,4,6-trinitrophenol (TNP) (98%), 1,3-dinitrobenzene (DNB) (97%), 2,4-dinitrotoluene (DNT) (97%), nitobenzene (NB) (99%), 4-nitrotoluene (NT) (99%) and benzene(B) (99%), were used as received from Sigma-Aldrich without further purification. The water used was double distilled and filtered through a Millipore membrane.

### Synthesis and initial characterizations

A reaction mixture of $Y(NO_3)_3.6H_2O$ (0.383 g, 1 mM) and 1,4-Phenylenediacetic acid (0.3001 g, 1.5 mM) along with 0.2 ml water and 0.05 ml ethanol was ground thoroughly in a mortar for one hour. The resulted colourless gel like product was heated at 180°C for 10 min. Light yellow coloured crystalline **1** were collected (yield ≈ 90%) after washing with sufficient quantity of water and diethyl ether. Similar procedure has also been used for the synthesis of the $Tb^{3+}$ doped compound (**Tb@1**) by replacing 10% of $Y^{3+}$ salt with $Tb^{3+}$ salt. The products were analyzed by Powder X-ray diffraction (XRD) in the 2θ range 5-50° using Cu Kα radiation (Rigaku, MiniFlex II). Single crystals of **1** were synthesized using solvothermal method. For this, a mixture of $Y(NO_3)_3.6H_2O$ (0.383 g, 1 mM), 1,4-Phenylenediacetic acid (0.2001 g, 1 mM), 8 ml water and 2 ml ethanol was reacted in a PTFE-lined acid digestion vessel (23 mL) at 180 ºC for 6 hours. Light yellow coloured brick shaped crystals of **1** were collected (yield ≈ 70%) after washing with sufficient quantity of water. The starting pH value and the pH value after the reaction were 1 and 3, repectively. Elemental analysis for **1** Calcd: C 44.55, H 3.71. Found: C 44.37, H 3.8; For Tb@**1** Calcd: C 43.79, H 3.64. Found: C 43.67, H 3.71 (values given in percentage). The powder XRD patterns of **1** and **Tb@1** being entirely consistent with the simulated XRD pattern generated based on the structures determined using the single-crystal XRD of bulk **1** (see ESI, Fig. S1)

### Instrumentations

The IR spectrum were recorded on a KBr pellet (Perkin-Elmer, SPECTRUM 1000). The thermogravimetric analysis (TGA) of **1** was carried out (Perkin-Elmer Diamond) in nitrogen atmosphere (flow rate) 20 mL/min) in the temperature range RT-900 °C (heating rate 10 °C/min). The differential scanning calorimetric (DSC) measurement of **1** were also performed in the temperature range of 25 -500 °C (heating rate = 10 °C/min) (TA Instrument, Q2000). The morphologies and the sizes of **1** and **Tb@1** synthesized though grinding methods were investigated using scanning electron microscope (QUANTA FEG250, FEI). The ratio of Tb and Y of **Tb@1** were determined using EDX analysis (EDAX, QUANTA 200).

### Single crystal X-ray diffractions

A suitable single crystal was carefully selected under a polarizing microscope and glued carefully to a thin glass fiber. The single crystal data of **1** were collected on a Bruker AXS smart Apex CCD diffractometer at 293(2) K. The X-ray generator was operated at 50 kV and 35 mA using Mo Kα (λ = 0.71073 Å) radiation. Data were collected with ω scan width of 0.3º. A total of 606 frames were collected in three different setting of φ (0, 90, 180º) keeping the sample-to-detector distance fixed at 6.03 cm and the detector position (2$\theta$) fixed at -25º. The data were reduced using SAINTPLUS,[12] and an empirical absorption correction was applied using the SADABS program.[13] The structure was solved and refined using SHELXL97[14] present in the WinGx suit of programs (Version 1.63.04a).[15] All the hydrogen atoms of the carboxylic acids were initially located in the difference Fourier maps, and for the final refinement, the hydrogen atoms were placed in geometrically ideal positions and held in the riding mode. Final refinement included atomic positions for all the atoms, anisotropic thermal parameters for all the non-hydrogen atoms, and isotropic thermal parameters for all the hydrogen atoms. Full-matrix least-squares refinement against $|F^2|$ was carried out using the WinGx package of programs.[15] Details of the structure solution and final refinements is given in Table S1 (see ESI). CCDC: 1014825 contain the crystallographic data for this paper. These data can be obtained free of charge from The Cambridge Crystallographic Data Center (CCDC) via www.ccdc.cam.ac.uk/data_request/cif.

### Pholtoluminescent based detection measurements

The photoluminescence properties of **Tb@1′** dispersed in acetonitrile were investigated at room temperature. The dispersions were prepared by introducing 2 mg of **Tb@1′** into 2.00 mL solvent and ultrasonic agitation for 1 hour and diluted to 10 mL before measuring the spectra. Photoluminescent spectra were measured using a PerkinElmer LS-55 spectrofluorometer. The analytes were added into the dispersion using micro pipette. UV-Vis spectra of analytes in acetonitrile solvent were studied using Shimadzu UV 3101PC spectrophotometer.

### Computational tools

The Gaussian 03 was used to carry out time dependent DFT calculations for the determination of optical gaps of the ligand and analytes using 6-311+g(d,p) basis sets.[16]

## Results and Discussion

### Structure and morphology

The single crystal X-ray diffraction studies reveal that the asymmetric unit of **1** consists of two $Y^{3+}$ ions, two full PDA, two half PDA, one coordinated water and two extra framework water molecules (see ESI, Fig. S2). The metal ion, Y(1), is surrounded by eight oxygen atoms of PDA and has a distorted a dodecahedron geometry. The metal ion, Y(2), is coordinated by eight oxygen atoms of PDA and one water molecule and has a distorted tricapped trigonal prismatic environment. The Y-O bonds have distances in the range of 2.242(3)-2.693(3) Å and the O-Y-O bond angles are in the range of 50.35(8)-165.42(10)°. The selected bond distances and angles for **1** are listed in Table S2 and S3, respective, in ESI. The Y(1) and Y (2) ions are bridged by carboxylato groups of PDA resulting in one-dimensional zigzag chains parallel to the *c* axis (see ESI, Fig. S3). The one-dimensional chains are connected with the PDA units to form three dimensional structures with one dimensional channels (ca. 9.45 × 19.64 $Å^2$ without water molecules) (Figure 1). The guest water molecules occupy the channels and the coordinated water molecules pointed towards the channels. The channels are lined with the π-electron rich benzene moiety of PDA, where the benzene rings are in both parallel and perpendicular to the channel wall. The similar structures were reported earlier based on pure lanthanide elements.[17]

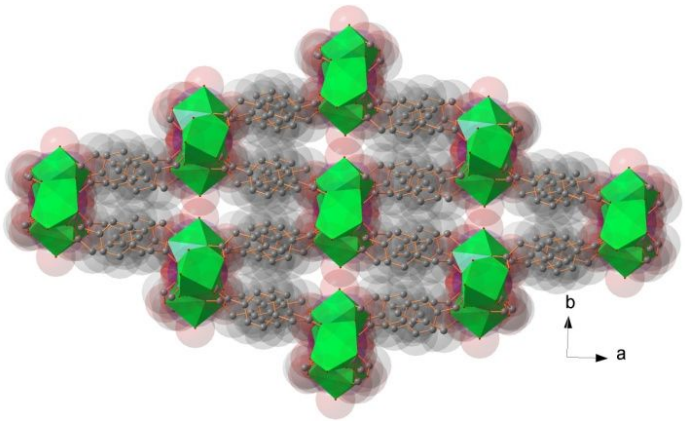


**Fig. 1.** View of three-dimensional connectivity between Y-polyhedra and PDA ligands in $[Y_2(PDA)_3(H_2O)_1].2H_2O$ (PDA = 1,4-Phenylenediacetate), **1**

The sizes and the morphologies of **1** and **Tb@1** were studied using scanning electron microscopy (SEM) (see ESI, Fig. S4). Powder grains of both the compounds are brick shaped with submicron size (Figure 2).

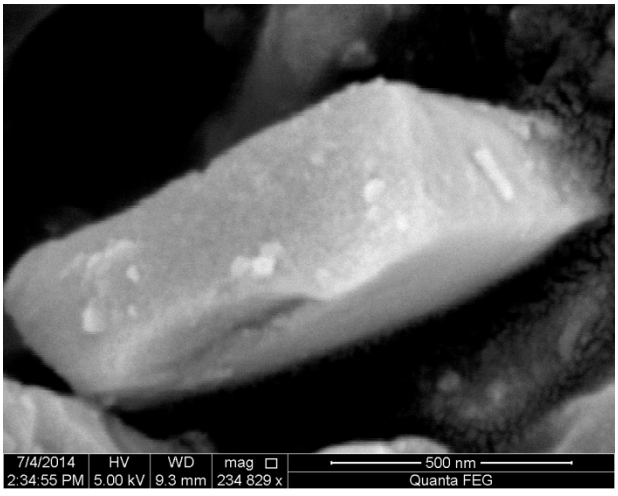


**Fig. 2.** SEM image of submicron sized crystal of **Tb@1**

These sizes have a significant impact on the homogeneous disperse ability on acetonitrile. The EDX analysis on several crystal of **Tb@1** shows the presence of Y and Tb with molar ratio of ~9:1 (see ESI, Fig. S5).

**Thermal Properties**

TGA show that **1** releases water molecules (both coordinated and extra-framework) upto 150 °C and the water free material could be obtained by direct heating of **1** at 200 °C for 2 h and retains the identical framework structure of **1**, which is confirmed by TGA (see ESI, Fig. S6) and PXRD (see ESI, Fig. S7). The DSC data show two endothermic peaks centered at 145 °C and 457 °C corresponding to removal of water molecules and decomposition of organic ligands, respectively (see ESI, Fig. S8).

**Nitro-explosive detections**

The guest free **Tb@1** (**Tb@1'**) when dispersed in acetonitrile exhibited strong emission in visible region upon excitation at 225 nm. The emission in higher energy (< 400 nm), generally observed due to π*→n and π*→π transitions of aromatic dicarboxylates, are excluded by using appropriate cut-off (see ESI, Fig. S9). The emission bands observed at 486, 541, 583 and 618 nm can be assigned to the $^5D_4 \rightarrow {}^7F_6$, $^5D_4 \rightarrow {}^7F_5$, $^5D_4 \rightarrow {}^7F_4$ and $^5D_4 \rightarrow {}^7F_3$ transitions, respectively, based on PDA sensitized $Tb^{3+}$ centered emission.[9b,9c] To explore the ability of **Tb@1'** to sense a trace amount of nitro explosives, luminescence quenching titrations were performed with incremental addition of analytes to **Tb@1'** dispersed in acetonitrile. Figure 3A shows changes in the luminescence intensity with the increasing addition of TNP (upto 100 μM). The visible bright green emission of **Tb@1'** on UV exposure vanished upon the addition of the TNP, which quenched nearly 96% of the initial luminescence intensity (based on the $^5D_4 \rightarrow {}^7F_5$ emission). To determine the detection limit, the titration has been performed using ultra low concentration of TNP. As can be seen from figure 3B, the luminescence quenching can be clearly detected at as low as 0.8 μM concentration which is equivalent to 0.18 ppm of TNP in acetonitrile.

Luminescence quenching titrations were also performed with other nitro aromatics such as 1,3-dinitro benzene (DNB), 2,4-dinitro toluene (DNT), nitro benzene (NB), 4-nitro toluene (NT) and non-nitro benzene (B) (see ESI, Fig.S10 – S14). Among these, DNT and DNB show similar and comparable luminescence quenching with TNP. With the incremental addition of DNT and DNB (100 μM) show nearly 89% and 92% quenching, respectively. NB and NT also shows small amount of quenching (NB>NT) whereas no quenching effect is observed in the case of benzene (B) (Figure 4). Similar luminescence quenching titrations with toluene and phenol also show negligible quenching behaviour (see ESI, Fig. S15 & S16)

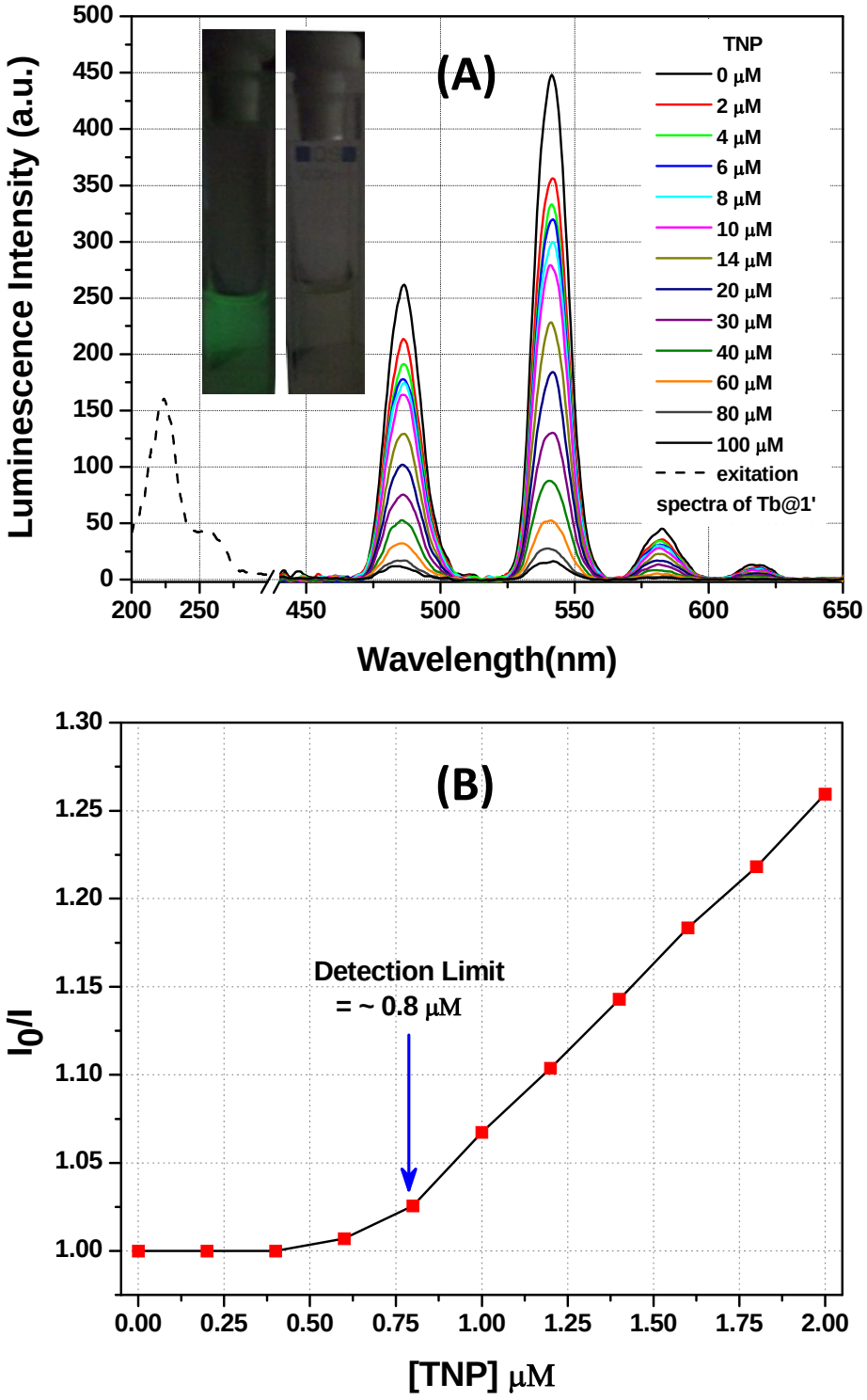


**Fig. 3.** (A) Emission spectra of **Tb@1'** dispersed in acetonitrile upon incremental addition of TNP solution ( $\lambda_{ex}$ = 225 nm). Final concentration of TNP in the medium is indicated in the legend. Black dashed curve is the excitation spectra **Tb@1'** in absence of TNP. Inset: a photograph showing the original luminescence of **Tb@1'** sample and the quenched one in presence of 100 μM TNP. (B) Luminescence quenching *vs* concentration of TNP plot (based on $^5D_4 \rightarrow {}^7F_5$ emission at 541 nm) indicating the detection limit. (where $I_0$ = luminescence intensity in absence of analyte, I = luminescence intensity with incremental addition of TNP).

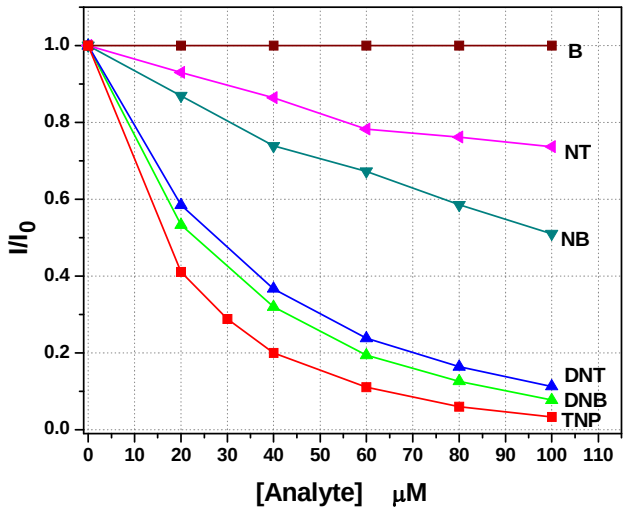


**Fig.4.** Plot of fraction of luminescence intensity of **Tb@1' (at 541 nm)** vs concentration of analytes. $I_0$ and I are luminescence intensity in absence and presence of analyte, respectively.

To understand the sensitivity, the Stern-Volmer plots were used to calculate the quenching constants of the analytes (Fig. 5) using the SV equation $(I_0/I) = K_{SV}[A] + 1$, where $I_0$ and I are the luminescence intensities before and after the addition of the analyte, [Q] is the molar concentration of the analyte and $K_{SV}$ is the quenching constant. As shown in fig. 5A, at low concentration (upto 20 μM) of all nitro analytes a linear increase in $(I_0/I)$ was observed. With the increasing of concentration SV plot diverged from linearity and began to bend upwards in the case of TNP, DNT and DNB (Fig. 5B). The linear variation at lower concentration are mainly due to static quenching, whereas the steep curves at higher concentration are presumably due to dynamic quenching. The static quenching can be accredited due to the ground state interaction between the analytes and the **Tb@1'**. The dynamic quenching are mainly due to the energy and electron transfer processes between the analytes and the **Tb@1'**. Apart from these mechanisms, absorption of excitation light by the analyte itself may also contribute to the quenching effect. Fitting of linear part of plots allows determination of the quenching constants ($K_{sv}$) to be 70920 $M^{-1}$ for TNP, 44000 $M^{-1}$ for DNB, 35430 $M^{-1}$ for DNT, 7690 $M^{-1}$ for NB and 3880 $M^{-1}$. The larger observed $K_{sv}$ values revealed extremely high sensitivity, which made **Tb@1'** one of the best sensitive luminescence based metal-organic detector for TNP, DNB and DNT.

The homogeneous dispersible nature of the submicron sized metal-organic materials has enabled a close contact between the **Tb@1'** and the analytes. In addition to this, the sufficient large one-dimensional channels of **Tb@1'** can permit easy diffusion of single six member ring based aromatic analytes in the electron rich framework. This enables proximity and molecular interaction between **Tb@1'** and analytes which result significant amount of static quenching. Apart from static quenching, the mechanism of the ligand sensitized metal centered luminescence quenching of **Tb@1'** in presence of analytes is primarily due to the reduction of amount of excitation energy required to sensitize the $Tb^{3+}$ activators. The excitation energy losses are attributed to the two possible mechanisms: (i) Absorption of the excitation energy by the analytes by competing with the PDA ligand, and (ii) Part of excitation energy used for the transfer of electron from the ligand excited state to the LUMO of the analytes. The schematic of the important energy/electron transfer processes are shown in Figure 6. The absorption spectra of the analytes in acetonitrile are informative to rationalize the observed luminescence quenching (see ESI, Fig. S17). TNP, DNB and DNT have similar absorption bands (~240 nm) which are closed to the excitation wavelength (225 nm) used for the emission studies.

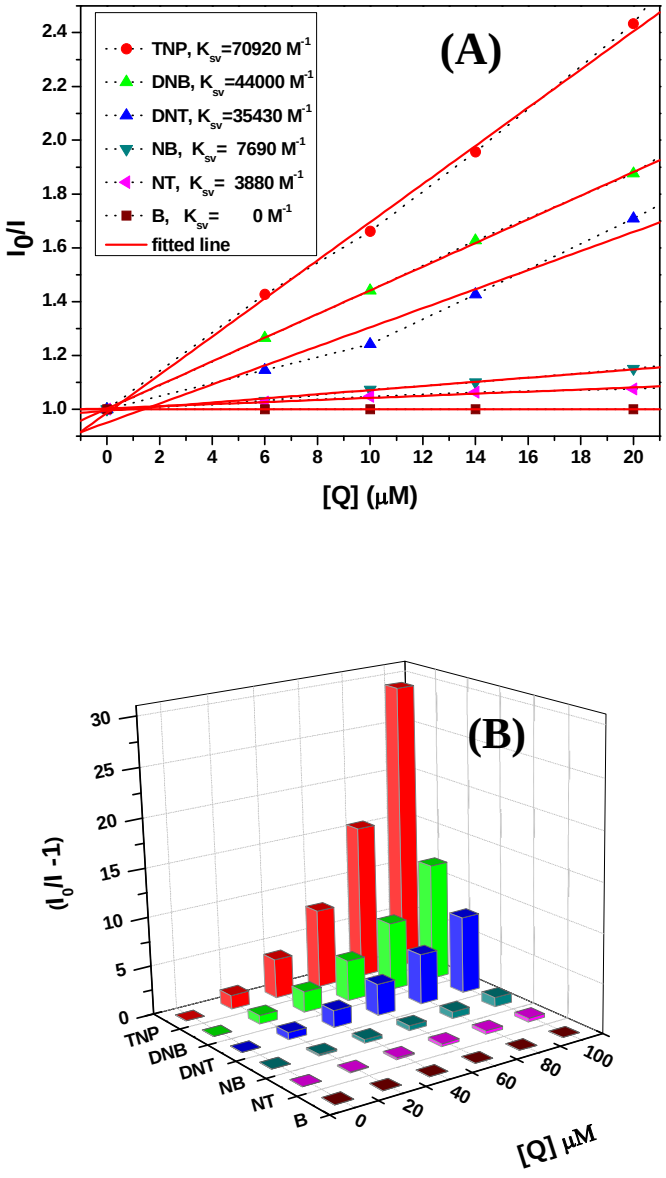


**Fig.5.** (A) Plot of $I_0/I$ of **Tb@1' (at 541 nm)** vs concentration of analytes in lower concentration range of analytes (upto 20 μM). $I_0$ and I are luminescence intensity in absence and presence of analyte, respectively. (B) Stern-Volmer plots of analytes in higher concentration range of analytes (upto 100 μM) .

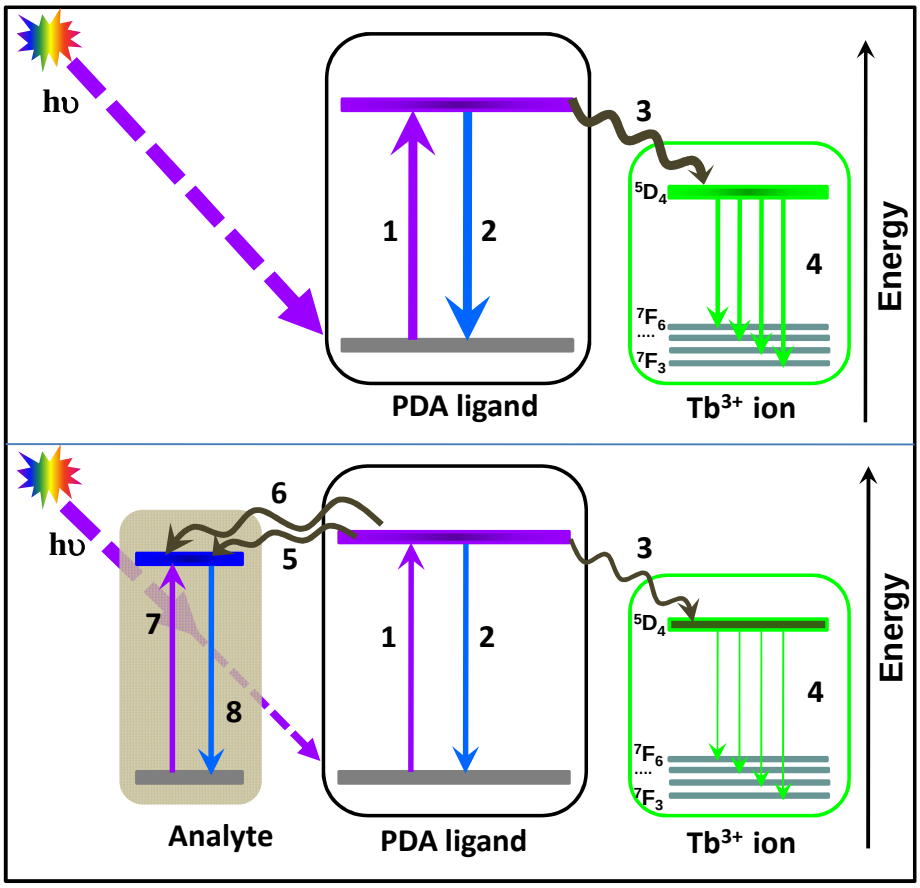


**Fig.6.** Schematic of various energy/electron transfer processes in absence of analyte (upper panel) and in presence of analyte (lower panel): **1**. UV light excite ligand centre; **2**. Ligand based luminescence; **3**. Energy transfer from ligand to $Tb^{3+}$ ions; **4**. Emission from $Tb^{3+}$ ions; **5**. Energy transfer from ligand to analyte; **6.** Electron transfer from ligand to analytes; **7**. Absorption of UV light by the analyte; **8.** Analyte based luminescence. Presence of analyte absorbs a part of hυ as well as reduce (due to **5** and **6**) the flow of energy from ligand centre to the metal centre, resulting large quenching of lumnisence.

This indicates the possibility of absorption of the excitation light by the analyte as well as the possibility of electron transfer from the excited ligand site to the slightly lower excited state of analyte (Figure 6). In addition to the band at ~240 nm, TNP has another absorption band centred at 350 nm which is overlapped to a good extent with the ligand centered emission (see ESI, Fig. S18). This overlap indicates the possibility of resonance energy transfer from the ligand site to TNP. In case of NB and NT, the absorption bands are longer in wavelength (peaks at 260 nm for NB and 275 nm for NT). This suggest that, both the processes (absorption and electron transfer) in these cases are not so favourable compared to the above three nitro aromatics. Benzene, on the other hand, does not have any absorption bands at longer wavelength than 225 nm resulting non quenching process. For static quenching as well as electron transfer and energy transfer processes (ligands to analytes)**,** close proximity of the detector and the analyte is the prerequisites. Close proximity indicates the molecular level interaction between the ligand moiety and the analytes. FTIR studies of the TNP soaked **Tb@1'** indicate the interaction between the ligand and the TNP (see ESI, Fig. S19).

To rationalize the experimental data, the optical gap of the optimized conjugated ligand moiety of the metal-organic materials and the analytes are calculated by time dependent density functional theory with basis set 6-311+g(d,p) using Gaussian 03 (see ESI, Table S4).[16] All the calculations are done on the optimised structure in gas phase. The calculated optical gap of the ligand moiety is nearly 5.76 eV, which is slightly more than the experimental value (excitation energy). This small change is due the metal bonding and solvent effect which have not been included in the calculation. All five nitro aromatics have possible optical transitions nearer to the excitation energy (225 nm) and at the higher wavelength region (ca. 265 nm for TNP). Benzene, on the other hand, does not have any optical transition at higher than 200 nm wavelength which supported the non quenching behaviour. These indicate that the gas phase calculation agrees our experimental data keeping in mind the effects of solvent and other factors arise in the condensed phase.

It is also significant to compare the quenching efficiency of **Tb@1'** with other state-of-art metal-organic materials discovered for the detection of nitro explosives in liquid phase. Ghosh and co-workers investigated the selective detection of TNP in liquid phase using two important metal-organic materials. It was shown that the luminescence of $[Cd(ndc)_{0.5}(pca)].xG$ (G = guest molecules, pca = 4-pyridinecarboxylic acid)[7i] was quenched by TNP in acetonitrile with $K_{SV}$ value of 35000 $M^{-1}$ and $Zr_6O_4(OH)_4(L)_6$ (L = 2-phenylpyridine-5,4'-dicarboxylate)[3a] detect TNP in aqueous phase with $K_{SV}$ value of 29000 $M^{-1}$. Zhou et al. reported detection of 2,4-DNT with $K_{SV}$ value of 1310 $M^{-1}$ using a Eu based MOF, $Eu_3(MFDA)_4(NO_3)(DMF)_3$ (MFDA = 9,9-dimethylfluorene-2,7-dicarboxylate) in DMF.[10b] Qian et el. have reported $Fe_3O_4$@Tb-BTC magnetic metal–organic nanospheres for the detection of nitro-



 

explosive in ethanol with $K_{SV}$ values of 25600 $M^{-1}$ for 2,4-DNT and 18390 $M^{-1}$ for TNP.[10a]

It is also appealing to compare with the conjugated organic molecules and polymers material reported in recent years for liquid phase detections of nitro explosive. Mukherjee and co-workers reported recently detection of TNP using electron rich supramolecular polymers of pyrene-based polycarboxylic acids along with their corresponding discrete esters in chloroform/DMSO. They have used six different but related compounds and the highest $K_{SV}$ value obtained in this study is 37824 $M^{-1}$.[18] They have also reported detection TNP using two different anthracene-functionalized tris-imidazolium salts in chloroform and the observed $K_{SV}$ values are 38000 and 33000 $M^{-1}$.[19] Patil and co-workers reported detection of TNP using π-conjugated fluoranthene derivative with $K_{SV}$ values 99000 $M^{-1}$ for TNP and 860 $M^{-1}$ for DNT ethanol.[20] An amine-functionalized mesoporous silica nanoparticles containing-poly(phenylenevinylene) (PPV@MSN-$NH_2$) was shown to detect DNT in ethanol with $K_{SV}$ value of 15500 $M^{-1}$ through fluorescence resonance energy transfer (FRET).[21] The above comparison indicate **Tb@1** is superior than all the metal-organic materials reported for the detection of TNP, DNB and DNT in liquid phase with respect of their quenching efficiency and it is also comparable to conjugated organic molecules and polymers.

## Conclusions

In conclusion, a luminescent submicron sized metal-organic material demonstrates high sensitive detection of TNP, DNB and DNT in acetonitrile through the quenching of organic ligand (PDA) sensitized $Tb^{3+}$ centered luminescence. Experimental and theoretical calculation explained that static quenching as well as the excitation energy absorption and electron transfers are the mechanisms for the reduction of luminescence intensity in presence of nitro aromatics. In case of TNP, additionally, the resonance energy transfer mechanism plays a significant role. Possibility of several quenching mechanisms makes our material more sensitive towards nitro explosives. The importance of present work for liquid phase detection of nitro explosive is many folds.

(1) Present work, for the first time demonstrates the potential of the use of f-electron based activator supported by non f-based [Y] metal-organic host for detection of nitro explosives where the self quenching, generally observed for pure Tb and Eu based compounds, is minimised.
(2) The large stokes shift [225 to 541 nm] make this materials an easy naked eye detector using UV light. Large number of reported explosive detectors are based on blue emission where it is very difficult to distinguish the bluish excitation light (UV) and the emission light through naked eye.
(3) The close interaction between the analytes and the materials in solution phase has been achieved due to submicron sizes of the material. The close contact between the analyte and the detector is important for luminescence based detection. Generally solution phase or solvothermally synthesized metal-organic materials suffered from their large sizes to become an efficient detector.

## Acknowledgements

This work was supported by DST INSPIRE faculty research grant (IFA12-CH-69). PM thanks Prof. A. K. Raychaudhuri and Dr. Barnali Ghosh, SNBNCBS and Prof. S. Natarajan, IISc for their support to execute this project. PM also thanks the DST for INSPIRE faculty award and Fast track project grant. MK thanks DST for UNANST computation facility and Sajeev Chacko. SKM thanks UGC for Start-Up-Grant (20-5(17)/2012(BSR), dt. 30/03/13). SKM also thanks Dr N A Begum for instrumental facility (DST Project: SR/SO/BB-0007/2011, dt. 21/08/12).

## Notes and references

[a]Department of Condensed Matter Physics and Material Sciences, S.N Bose National Centre for Basic Sciences, JD Block, Sector III, Salt Lake City, Kolkata -700098, India. Email: partha.mahata@bose.res.in
[b]Framework solids Laboratory, Solid State and Structural Chemistry Unit, Indian Institute of Science, Bangalore-560012, India
[c]Department of Chemistry, Siksha-Bhavana, Visva-Bharati University, Santiniketan-731235, West Bengal, India. Email: sudip.mondal@visva-bharati.ac.in

† Crystal data for **1**: $[Y_2\{C_8H_8(COO)_2\}_3(H_2O)]\cdot 2H_2O$, M = 808.36, monoclinic, space group $P2_1/n$ (no. 14), a = 21.625 (3), b = 10.0060 (13), c = 14.0570 (17) Å, β = 91.401 (7); V= 3040.8 (6) $Å^3$, Z = 4, $\rho_{cal}$ = 1.766 g $cm^{-3}$, $\mu(Mo_{k\alpha})$ = 3.874 $mm^{-1}$, 27938 reflections, 7009 unique ($R_{int}$ = 0.0775), 4658 observed I>2σ(I), $R_1$ = 0.0905, $wR_2$ = 0.0940 and GOF = 0.999 for 448 parametersFootnotes should appear here.
Electronic Supplementary Information (ESI) available: [Details of the experimental and computational data]. See DOI: 10.1039/b000000x/

1. (a) S.-R. Zhang, D.-Y. Du, J.-S. Qin, S.-J. Bao, S.-L. Li, W.-W. He, Y.- Q. Lan, P. Shen and Z.-M. Su, *Chem. Eur. J.*, 2014, **20,** 3589; (b) S. J. Toal and W. C. Trogler, *J. Mater. Chem.*, 2006, **16**, 2871; (c) M. E. Germain and M. J. Knapp, *Chem. Soc. Rev.*, 2009, **38**, 2543; (d) Y. Salinas, R. Martinez-Manez, M. D. Marcos, F. Sancenon, A. M. Costero, M. Parra and S. Gil, *Chem. Soc. Rev.*, 2012, **41**, 1261.
2. S.W. Thomas, G. D. Joly and T. M. Swager, *Chem. Soc. Rev.*, 2007, **36,** 1339
3. (a) S. S. Nagarkar, A. V. Desai and S. Ghosh, *Chem. Commun.*, 2014, **50**, 8915; (b) G. He, H. Peng, T. Liu, M. Yang, Y. Zhang and Y. Fang, *J. Mater. Chem.*, 2009, **19,** 7347.
4. B. Roy, A. K. Bar, B. Gole and P. S. Mukherjee, *J. Org. Chem.*, 2013, **78**, 1306.
5. H. Sohn, M. J. Sailor, D. Magde and W. C. Trogler, *J. Am. Chem. Soc.*, 2003, **125**, 3821.
6. (a) D. Li, J. Liu, R. T. K. Kwok, Z. Liang, B. Z. Tang and J. Yu, *Chem. Commun.*, 2012, **48,** 7167; (b) E. S. Snow, F. K. Perkins, E. J. Houser, S. C. Badescu and T. L. Reinecke, *Science*, 2005, **307,** 1942; (c) B. Gole, S. Shanmugaraju, A. K. Bar and P. S. Mukherjee, *Chem. Commun.*, 2011, **47,** 10046; (d) S. Shanmugaraju, S. A. Joshi and P. S. Mukherjee, *Inorg. Chem.*, 2011, **50,** 11736; (e) K. K. Kartha, S. S. Babu, S. Srinivasan and A. Ajayaghosh, *J. Am. Chem. Soc.*, 2012, **134,** 4834.
7. (a) Z. Hu, B. J. Deibert and J. Li, *Chem. Soc. Rev.*, 2014, **43**, 5815; (b) A. Lan, K. Li, H. Wu, D. H. Olson, T. J. Emge, W. Ki, M. Hong and J. Li, *Angew. Chem. Int. Ed.*, 2009, **48,** 2334; (c) S. Pramanik, C. Zheng, X. Zhang, T. J. Emge, J. Li, *J. Am. Chem. Soc.*, 2011, **133**, 4153; (d) K. C. Stylianou, R. Heck, S. Y. Chong, J. Bacsa, J. T. A. Jones, Y. Z. Khimyak, D. Bradshaw, M. J. Rosseinsky, *J. Am. Chem. Soc.*, 2010, **132**, 4119; (e) D. Liu, K. Lu, C. Poon and W. Lin, *Inorg. Chem.*, 2014, **53**, 1916; (f) T. K. Kim, J. W. Lee, D. Moon, H. R. Moon, *Inorg. Chem.*, 2013, **52**, 589; (g) C. Wang and W. Lin, *J. Am.*

*Chem. Soc.*, 2011, **133**, 4232; (h) B. Chen, L. Wang, F. Zapata, G. Qian, E. B. Lobkovsky, *J. Am. Chem. Soc.*, 2008, **130**, 6718; (i) S. S. Nagarkar, B. Joarder, A. K. Chaudhari, S. Mukherjee and S. K. Ghosh, *Angew. Chem., Int. Ed.*, 2013, **52**, 2881; (j) B.Gole, A. K. Bar and P. S. Mukherjee, *Chem. Eur. J.*, 2014, **20,** 2276; (k) G.-Y. Wang, C. Song, D.-M. Kong, W.-J. Ruan, Z. Chang, and Y. Li, *J. Mater. Chem. A,* 2014, **2,** 2213; (l) B. Gole, A. K. Bar and P. S. Mukherjee, *Chem. Commun.*, 2011, **47**, 12137; (m) Z. Zhang, S. Xiang, X. Rao, Q. Zheng, F. R. Fronczek, G. Qian and B. Chen, *Chem. Commun.*, 2010, **46,** 7205; (n) C. Zhang, Y. Che, Z. Zhang, X. Yang and L. Zang, *Chem. Commun.*, 2011, **47,** 2336

8. H. Xu, F. Liu, Y. Cui, B. Chen and G. Qian, *Chem. Commun.*, 2011, **47,** 3153.
9. (a) R. C. Powell and Z. G. Soos, *Phys. Rev B*, 1972, **5**, 1547; (b) P. Mahata, K. V. Ramya and S. Natarajan, *Chem. Eur. J.*, 2008, **14**, 5839; (c) P. Mahata, K. V. Ramya and S. Natarajan, *Dalton Trans.*, 2007, 4017.
10. (a) J. –J. Qian, L. –G. Qiu, Y. –M. Wang, Y. –P. Yuan, A. –J. Xie and Y. –H. Shen, *Dalton Trans.*, 2014, **43**, 3978; (b) X. Zhou, H. Li, H. Xiao, L. Li, Q. Zhao, T. Yang, J. Zuo and W. Huang, *Dalton Trans.*, 2013, **42**, 5718.
11. R. Li, Y.- P. Yuan, L. –G. Qiu, W. Zhang and J. –F. Zhu, *Small*, 2012, **8**, 225.
12. SMART (V 5.628), SAINT (V 6.45a), XPREP, SHELXTL, Bruker AXS Inc., Madison, Wisconsin, USA, 2004.
13. G. M. Sheldrick, *Siemens area correction absorption correction program, University of Göttingen, Göttingen, Germany, 1994*.
14. G. M. Sheldrick, *SHELXL-97 program for crystal structure solution and refinement, University of Göttingen, Göttingen, Germany, 1997*.
15. J. L. Farrugia, *WinGx suite for small-molecule single crystal crystallography*. *J. Appl. Crystalogr*. 1999, **32**, 837.
16. M. J. Frisch, G. W. Trucks, H. B. Schlegel, G. E. Scuseria, M. A. Robb, J. R. Cheeseman, J. A. Montgomery, Jr., T. Vreven, K. N. Kudin, J. C. Burant, J. M. Millam, S. S. Iyengar, J. Tomasi, V. Barone, B. Mennucci, M. Cossi, G. Scalmani, N. Rega, G. A. Petersson, H. Nakatsuji, M. Hada, M. Ehara, K. Toyota, R. Fukuda, J. Hasegawa, M. Ishida, T. Nakajima, Y. Honda, O. Kitao, H. Nakai, M. Klene, X. Li, J. E. Knox, H. P. Hratchian, J. B. Cross, C. Adamo, J. Jaramillo, R. Gomperts, R. E. Stratmann, O. Yazyev, A. J. Austin, R. Cammi, C. Pomelli, J. W. Ochterski, P. Y. Ayala, K. Morokuma, G. A. Voth, P. Salvador, J. J. Dannenberg, V. G. Zakrzewski, S. Dapprich, A. D. Daniels, M. C. Strain, O. Farkas, D. K. Malick, A. D. Rabuck, K. Raghavachari, J. B. Foresman, J. V. Ortiz, Q. Cui, A. G. Baboul, S. Clifford, J. Cioslowski, B. B. Stefanov, G. Liu, A. Liashenko, P. Piskorz, I. Komaromi, R. L. Martin, D. J. Fox, T. Keith, M. A. Al-Laham, C. Y. Peng, A. Nanayakkara, M. Challacombe, P. M. W. Gill, B. Johnson, W. Chen, M. W. Wong, C. Gonzalez, J. A. Pople, *Gaussian 03*, Revision B.05, Gaussian, Inc., Pittsburgh, PA, USA, 2003.
17. L. Pan, K. M. Adams, H. E. Hernandez, X Wang, C. Zheng, Y. Hattori, K. Kaneko, *J. Am. Chem. Soc.*, 2003, **125**, 3062.
18. B. Gole, W. Song, M. Lackinger and P. S. Mukherjee, *Chem. Eur. J.*, 2014, **20**, DOI: 10.1002/chem.201403345
19. B. Roy, A. K. Bar, B. Gole and P. S. Mukherjee, *J. Org. Chem.*, 2013, **78**, 1306.
20. N. Venkatramaiah, S. Kumar and S. Patil, *Chem. Commun.*, 2012, **48**, 5007.
21. L. Feng, H. Li, Y. Qu and C. Lü, *Chem. Commun.*, 2012, **48**, 4633.